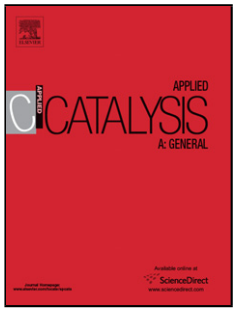

Etherification of biomass-derived furanyl alcohols with aliphatic alcohols over silica-supported nickel phosphide catalysts: Effect of surplus P species on the acidity

Mi Shin (Data curation) (Formal analysis) (Investigation) (Methodology) (Validation)<ce:contributor-role>Writing -original draft) (Visualization), Jinsung Kim (Formal analysis) (Investigation), Young-Woong Suh (Conceptualization) (Funding acquisition) (Project administration) (Supervision) (Writing - review and editing)

PII: S0926-860X(20)30356-2

DOI: https://doi.org/10.1016/j.apcata.2020.117763

Reference: APCATA 117763

To appear in: *Applied Catalysis A, General*

Received Date: 1 June 2020

Revised Date: 10 July 2020

Accepted Date: 23 July 2020

Please cite this article as: { doi: https://doi.org/

Etherification of biomass-derived furanyl alcohols with aliphatic alcohols over silica-supported nickel phosphide catalysts: Effect of surplus P species on the acidity

Mi Shin,[a] Jinsung Kim,[a] and Young-Woong Suh[a,b,*]

[a]Department of Chemical Engineering, Hanyang University, Seoul 04763, Republic of Korea

[b]Research Institute of Industrial Science, Hanyang University, Seoul 04763, Republic of Korea

*Corresponding author. *E-mail address:* ywsuh@hanyang.ac.kr (Y.-W. Suh)

Graphical Abstract

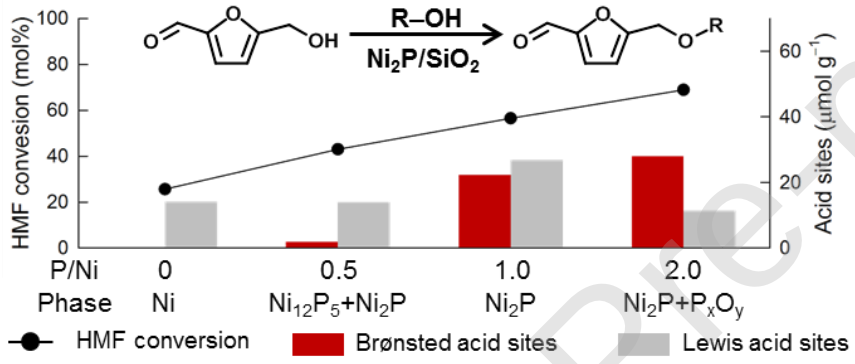

Highlights

- Ni_2P/SiO_2 catalysts are capable of etherifying HMF with aliphatic alcohols.
- Furanyl alcohols can be etherified with ethanol over Ni_2P/SiO_2.
- The P–OH group could be located on the surface of Ni_2P particles and SiO_2 support.
- The Brønsted acidity of Ni_2P/SiO_2 is associated with the surplus P species.
- Both Brønsted and Lewis acid sites contribute to the activity of Ni_2P/SiO_2.

Abstract

The acidity of nickel phosphide (Ni_2P) catalysts plays a crucial role in producing a desired hydrodeoxygenation molecule from biomass-derived substrates; yet, it has never been explored in acid-catalyzed reactions. Herein, we demonstrated the activity of silica-supported Ni_2P catalyst prepared with the nominal P/Ni ratio of 2 (Ni_2P/SiO_2-2P) in the etherification of furanyl alcohols (particularly, 5-(hydroxymethyl)furfural) with aliphatic alcohols including ethanol. By comparing the characteristics of Ni/SiO_2, P_xO_y/SiO_2, and Ni_2P/SiO_2-xP (x = 0.5 and 1), Ni_2P/SiO_2-2P was revealed to contain the Brønsted and Lewis acid sites of which both contributed to the etherification reaction. Notably, the Brønsted acidity was associated with the surplus P species added to produce the Ni_2P phase. Consequently, supported Ni_2P catalysts can work in acid-catalyzed reactions if an adequate ratio of Brønsted to Lewis acid sites is provided by the amount of the surplus P species determined by adjusting the P/Ni ratio.

Keywords: Etherification; Furanyl alcohol; Aliphatic alcohol; Nickel phosphide; Acidity

1. Introduction

Since the first report of Sweeny et al. in 1958 that nickel phosphide (Ni_2P) could catalyze the reduction of nitrobenzene to aniline [1], Ni_2P catalysts have been used for a great number of hydroprocessing reactions. Their representative applications are hydrodenitrogenation (HDN), hydrodesulfurization (HDS), and hydrodeoxygenation (HDO) that are essential in the production of ultra clean motor fuels by removing heteroatom-containing molecules from conventional fossil fuel and renewable biomass feedstock [2–4]. By virtue of unique performance of Ni_2P catalysts, extensive effort has been exerted to synthesize Ni_2P nanoparticles that are unsupported or often loaded onto various support materials [5].

Particularly, numerous studies have revealed a bifunctional character of supported Ni_2P affecting the product selectivity. The HDN and HDS reactions undergo hydrogenation on metallic Ni site and protonation on acid site of Ni_2P catalyst. Imporatnatly, the activity is correlated with a density of the Brønsted acid site originating from the P–OH group present

in the surface of Ni_2P [6–8]. The bifunctionality of Ni_2P is more vivid in the HDO reaction of biomass-derived chemicals because the removal of O is absolutely associated with acid site. In the case of guaiacol that is a phenolic model compound for lignin, benzene was preferentially formed over Ni_2P/SiO_2 at higher space times because the Brønsted acid site adjacent to Ni site could facilitate the dehydroxylation of phenol by protonating the oxygen in phenol [9,10]. Moreover, supported Ni_2P catalysts enabled selective transformation of cellulose into sorbitol: the acidity and metallic site were responsible for the hydrolysis of cellulose to glucose and subsequent hydrogenation of glucose to sorbitol, respectively [11,12]. In recent years, the HDO reaction of furfural, which is the dehydration product from xylose, was studied over Ni_2P catalysts. Jiménez-Gómez et al. reported high selectivity towards 2-methylfuran over Ni_2P/SiO_2, which is caused by the hydrogenation capacity of Ni site in the conversion of furfural to furfuryl alcohol that is coupled with the hydrogenolysis function of acid site in the subsequent transformation to 2-methylfuran [13]. Therefore, the acidity of Ni_2P catalysts clearly affects their HDO performance.

While understanding the catalytic actions of Ni_2P, we realized that the performance was determined only under H_2-rich conditions in order to assess superior hydrotreating ability. If it is true that Ni_2P contains the acidity, then it should display an activity in acid-catalyzed reactions taking place under inert atmosphere. Yet, this attempt has never been explored so far as we know. In literature we found a report that the conversion of furfural to 2-methylfuran over unsupported Ni_2P involves a step of the condensation of furfuryl alcohol into difurfuryl ether [14]. Although the authors employed HDO conditions for this transformation, their results prompted us to certify the capability of Ni_2P to catalyze an acidity-demanding reaction. In this context, the target reaction is etherification of furfuryl alcohols with aliphatic alcohols. Typically, 5-(hydroxymethyl)furfural (HMF), formed by dehydration of hexose sugars [15,16], can be etherified to 5-(alkoxymethyl)furfural that can be used as additive and precursor of drop-in fuel; for instance, the etherification product from HMF and ethanol, that is, 5-(ethoxymethyl)furfural (EMF) has a comparable energy density (8.7 kWh L^{-1}) to gasoline (8.8 kWh L^{-1}) and diesel (9.7 kWh L^{-1}) [17].

The catalyst employed for the etherification reaction is SiO_2-supported Ni_2P (Ni_2P/SiO_2) with the nominal P/Ni molar ratio of 2. Note that as the support acidity may initiate the reaction [18], SiO_2 is selected as a support due to no apparent activity. We have examined the catalytic behavior of Ni_2P/SiO_2 under H_2 for the conversion of HMF in the solvent of

tetrahydrofuran (THF) or ethanol. The etherification performance of Ni_2P/SiO_2 is confirmed under inert N_2 in the reaction of HMF with ethanol, and furthermore in the reactions involving other furanyl alcohols and aliphatic alcohols. The characteristics of the prepared Ni_2P/SiO_2 are investigated and compared with the samples prepared with different P/Ni ratios of 0.5 and 1 in order to find out the origin of acidity. Finally, catalyst recyclability and regeneration are examined for the etherification reaction.

2. Experimental

2.1. Catalyst preparation

The Ni_2P/SiO_2 catalyst with the nominal P/Ni ratio of 2, which is named Ni_2P/SiO_2-2P, was prepared by temperature-programmed reduction (TPR). Typically, an aqueous solution of $Ni(NO_3)_2{\cdot}6H_2O$ (1.25 g; 97%, Daejung Chemical) was first precipitated by adding a solution of $(NH_4)_2HPO_4$ (1.14 g; 98%, Sigma-Aldrich). After dissolving the precipitate by 10 wt% nitric acid, a SiO_2 support with the surface area of 350 $m^2\ g^{-1}$ (2 g; Alfa Aesar) was added, followed by aging for 2 h under vigorous stirring. The catalyst precursor was dried at 105 °C, calcined at 500 °C for 3 h, and finally reduced under H_2 (99.9%) at a flow rate of 200 mL min^{-1} in a quartz tube according to the following program: heating from 25 °C to 350 °C at a rate of 3.5 °C min^{-1}, further to 700 °C at 1 °C min^{-1}, and holding at 700 °C for 1 h. After cooling to 25 °C under N_2, the sample was finally obtained after passivation at 25 °C under N_2 gas flow for 1 h. In addition, Ni_2P/SiO_2-0.5P and Ni_2P/SiO_2-1P were prepared using the above recipe except the nominal P/Ni ratio being 0.5 and 1, respectively.

For comparison, several reference catalysts were prepared. Bulk (or unsupported) Ni_2P was prepared by reduction of commercial Ni_2P (Sigma-Aldrich; ~100 mesh) under a H_2 flow of 200 $cm^3\ min^{-1}$ using the temperature program identical to that employed for Ni_2P/SiO_2. A SiO_2-supported Ni catalyst (Ni/SiO_2) was prepared by wet impregnation, where the nominal Ni loading was 10 wt% which is identical to that in Ni_2P/SiO_2. SiO_2 (2 g) was added to an aqueous solution of $Ni(NO_3)_2{\cdot}6H_2O$ (1.10 g) in distilled water (30 mL). Then, the solution was aged for 2 h under vigorous stirring, followed by water evaporation. The sample was dried at 105 °C for 12 h and subsequently calcined at 500 °C for 3 h in an air flow of 100 mL min^{-1}. Finally, H_2 reduction was carried out using the same procedure as that employed for Ni_2P/SiO_2. On the other hand, a SiO_2-supported phosphate catalyst (P_xO_y/SiO_2) with the nominal P loading of 10 wt% was prepared by the method analogous to Ni/SiO_2 except the use of $(NH_4)_2HPO_4$ instead Ni source without a step of H_2 reduction.

As ion-exchange resin catalyst, Amberlyst 15 (4.7 meq g^{-1}) was kindly provided by Dow Chemical in Korea, while Nafion NR50 (0.8 meq g^{-1}) was purchased from Sigma-Aldrich.

2.2. Catalyst characterization

Powder X-ray diffraction (XRD) analysis was conducted using a Rigaku MiniFlex600 with a GADDS diffractometer using a Cu Kα radiation of 40 kV and 40 mA with a scan speed of 10° min^{-1} and a step size of 0.02°. The crystallite size was calculated using the Scherrer equation $D_p = K\lambda/\beta\cos\theta$, where D_p is the particle size in a unit of Å, K is the shape factor (0.94 in this study), λ is the wavelength of the X-rays, β is the full width at half maximum, and θ is the Bragg angle. The transmission electron microscopy (TEM) images were taken with a JEOL JEM 2100F microscope operating at 200 kV. The specific surface area and pore volume were measured using a Micromeritics 3Flex instrument at −196 °C with N_2 after degassing at 105 °C for 1 h under vacuum. X-ray photoelectron spectroscopy (XPS) was performed using a Thermo Fisher Scientific Messtechnik K-Alpha+ spectrometer with an Al Kα radiation of 1486.6 eV. The actual elemental compositions were obtained by an inductively coupled plasma atomic emission spectroscopy (ICP-AES) using a PerkinElmer Optima 8300 spectrometer operated with an RF generator power of 13000 W, RF frequency of 40 MHz, plasma gas flow of 12 L min^{-1}, auxiliary gas flow of 0.2 L min^{-1}, and nebulizer gas flow of 0.55 L min^{-1}. Prior to ICP-AES measurement, a sample of 0.03 g was mixed with a mixture of nitric acid (4 mL), hydrofluoric acid (4 mL), and perchloric acid (1 mL) over a hot plate, followed by dilution with water of 20 mL.

Pyridine-chemisorbed FT-IR analysis was performed to quantitatively measure the Brønsted and Lewis acid sites. The probe molecule was adsorbed in a Specac HTHP cell coupled with a Thermo Scientific Nicolet 6700 spectrometer with an MCT-A detector. The self-supporting disc of a sample (20 mg) was treated at 300 °C for 1 h in a vacuum of 1×10^{-3} mbar and then pyridine of 5 μL was directly injected at 100 °C. After degassing at 100 °C for 30 min, IR spectra were recorded with a scan number of 32 and a resolution of 4 cm^{-1}.

2.3. Activity test

The furanyl alcohols employed in this work are HMF, furfuryl alcohol (98%), and 5-methylfurfuryl alcohol (97%) purchased from Sigma-Aldrich, TCI Chemical, and Acros Organics, respectively. Also, a solution of 2,5-bis(hydroxymethyl)furan in ethanol was prepared by the hydrogenation of HMF over Cu/Al_2O_3 catalyst at 70 °C for 3 h, resulting in a

purity of over 99% (confirmed by gas chromatography (GC) measurement). The alcohol solvents are methanol (99.9%, J.T. Baker), ethanol (99.9%, Daejung Chemical), 1-propanol (99%, Samchun Chemicals), 2-propanol (99.5%, Daejung Chemical), *tert*-butanol (99.5%, Daejung Chemical), and 1-hexanol (98%, TCI Chemical).

For catalytic experiments, a stainless-steel batch reactor of 100 mL (Parr Instrument) was charged with a catalyst (100 mg), furanyl substrate, and solvent (19 mL) in which the substrate concentration was set at 0.21 M. The reactor was then purged with inert N_2 at 25 °C for 1 h and heated to a desired temperature (usually, 150 °C). The reaction started with stirring at 600 rpm and was performed for 3 h. After the reaction was complete, the heating and stirring were stopped and cooled to 25 °C. From the collected etherification product mixture, a sample (1.5 mL) was taken and then mixed with 0.08 g of toluene (99.5%) that is an external standard for GC analysis using an Agilent 7890A GC with a flame ionization detector (FID) and a INNOWAX capillary column (30 m × 0.25 mm × 0.25 μm). While the injector and detector were set at 250 and 300 °C, respectively, the oven temperature was programmed as follows: 40 °C for 2 min, ramping to 160 °C at 20 °C min^{-1}, holding at 160 °C for 2 min, followed by ramping to 250 °C at 10 °C min^{-1}, and finally holding at 250 °C for 5 min. The product was confirmed by GC-MS analysis (Agilent INNOWAX column). For quantitative measurement, the experiments were repeated at least three times and the average product compositions were reported in this context. Finally, the conversion of furanyl alcohol and the selectivity and yield of each product were calculated as follows:

$$\text{Conversion of furanyl alcohol (mol\%)} = \frac{(\text{mole of furanyl alcohol converted})}{(\text{mole of initial furanyl alcohol})} \times 100$$

$$\text{Product selectivity (mol\%)} = \frac{(\text{mole of the etherification product formed})}{(\text{mole of the total products formed})} \times 100$$

$$\text{Product yield (mol\%)} = \frac{(\text{mole of the etherification product formed})}{(\text{mole of initial furanyl alcohol})} \times 100$$

3. Results and discussion

3.1. Etherification activity of Ni_2P/SiO_2-2P catalyst

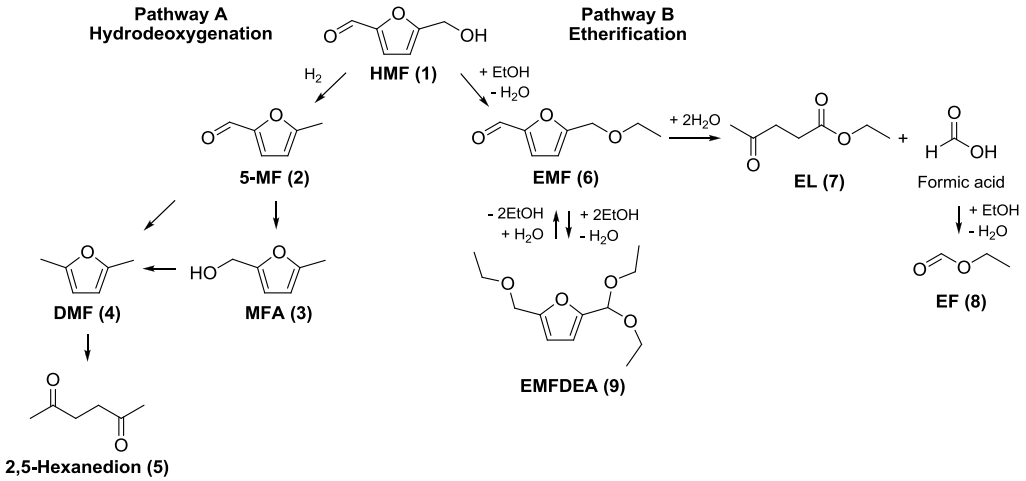

Scheme 1. Reaction pathway for conversion of HMF via hydrodeoxygenation (Pathway A) and etherification (Pathway B).

We examined the catalytic action of Ni_2P/SiO_2-2P in THF at 50 bar H_2 and 210 °C. As displayed in Fig. 1a, the products formed are 5-methylfurfural (5-MF) and 2,5-dimethylfuran (DMF) produced by the hydrodeoxygenation of HMF (Pathway A in Scheme 1) [13,19,20]. These HDO products were also found in the experiment at 240 °C showing the HMF conversion of 74.5% that is higher than 47.7% at 210 °C (Fig. 1b). However, they were not observed in the majority when the solvent was changed to ethanol. Instead, different GC peaks (marked by the asterisk in Fig. 1a) were detected from the products obtained by the tests at 210 and 240 °C. Based on GC-MS analysis of several authentic samples, the major products could be assigned to EMF and its acetalization product, 5-(ethoxymethyl)furfural diethyl acetal (EMFDEA), along with ethyl levulinate (EL) and ethyl formate (EF) in minor. These originate from the etherification of HMF with the solvent ethanol [21–24], as depicted in the Pathway B in Scheme 1. Quantitative results indicate that the conversion of HMF is 96.7% and 99.8% with the yield of all etherification products corresponding to 88.3% and 85.2% at 210 and 240 °C, respectively. The larger HMF consumption in ethanol than in THF is caused by the preferred etherification reaction over Ni_2P/SiO_2-2P. Besides, intermolecular dehydration of ethanol to diethyl ether (DEE) could occur.

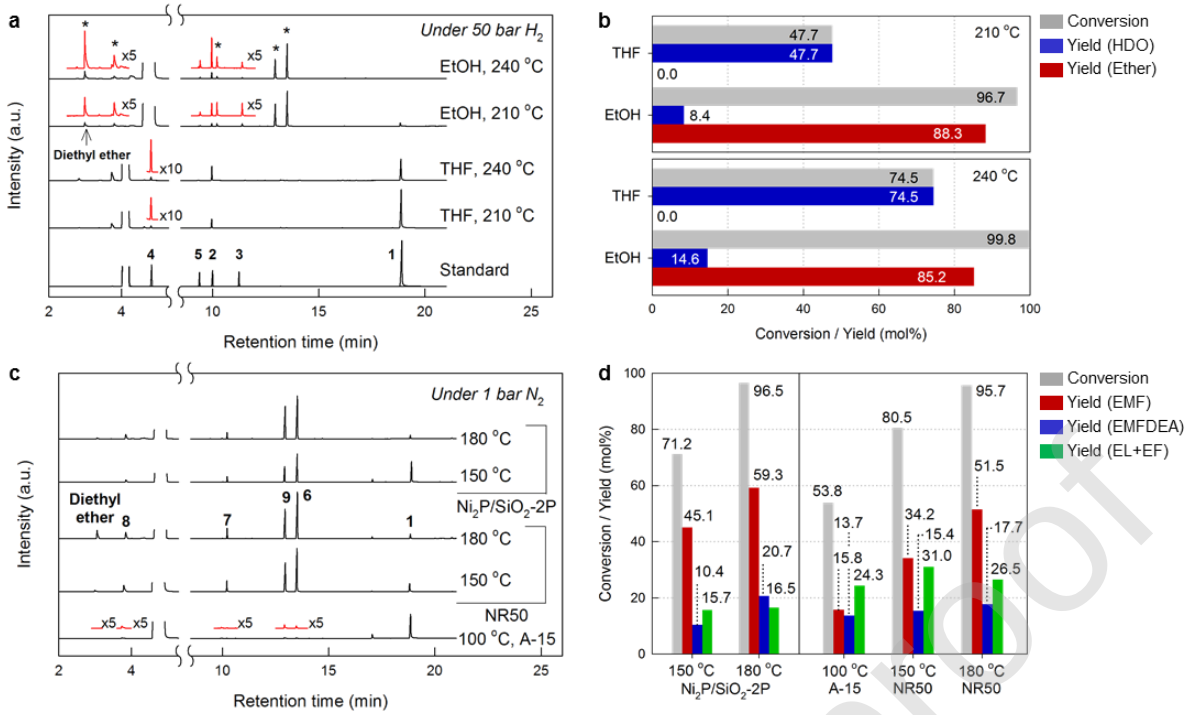

Figure 1. Conversion of HMF over Ni_2P/SiO_2-2P. a Gas chromatograms of the product mixtures obtained with a solvent of tetrahydrofuran (THF) and ethanol (EtOH) under the reaction conditions: catalyst 100 mg, HMF 4 mmol, solvent 19 mL, 210 and 240 °C, 50 bar H_2, and 3 h. **b** HMF conversion and product yields by the HDO and etherification pathways, calculated on the basis of the results in panel **a**. **c** Gas chromatograms of the product mixtures obtained using ethanol at 1 bar N_2 with different catalysts such as Ni_2P/SiO_2-2P (100 mg) at 150 and 180 °C, Amberlyst 15 (A-15, 0.6 mg) at 100 °C, and Nafion NR50 (NR50, 3.6 mg) at 150 and 180 °C under the reaction conditions: HMF 4 mmol, ethanol 19 mL, and 3 h. **d** HMF conversion and yields of etherification products (EMF, EMFDEA, and EL+EF), calculated on the basis of the results in panel **c**.

Additional tests were carried out at low temperatures (e.g., below 200 °C) under N_2 due to the aforementioned reaction conditions suitable for the HDO reaction. The catalyst loading used was determined based on the molar density of Brønsted acid site (BAS) relative to the initial mole of HMF; the ratio of BAS to HMF was 0.07%. Figure 1c exhibits that Ni_2P/SiO_2-2P catalyzes only the etherification reaction between HMF and ethanol at 150 and 180 °C. The yield of EMF was higher at 180 °C owing to the nearly complete conversion of HMF while the formation of EMF was more selective as 63.3% at 150 °C (Fig. 1d). When the BAS/HMF ratio increased to 0.14% and 0.50%, the HMF conversion at 150 °C was enhanced to 73.0% and 86.0%, respectively (Entries 6 and 7 in Table 1). However, the selectivity of EMF was reduced to 56.9% and 48.0% at 0.14% and 0.50% BAS/HMF, respectively. This suggests that the conversion of EMF into EL via hydration and further into EF via esterification can occur over Ni_2P/SiO_2-2P under the employed reaction conditions.

For comparison, we tested the two well-known ion-exchange resins, Amberlyst 15 (4.7 meq H^+ per gram) and Nafion NR50 (0.8 meq H^+ per gram), as solid catalyst because the etherification reaction proceeds by the protons tethered to the resin. Note that the relative concentration of proton to HMF ([H^+]/[HMF]), which is equivalent to the BAS/HMF ratio of Ni_2P/SiO_2-2P, was set at 0.07% for activity tests. First, when Amberlyst 15 was tested under N_2 at 100 °C, the HMF conversion was measured to be 53.8% even though the employed reaction temperature was as low as 100 °C due to low thermal stability (Table 1). However, EL and EF were produced in larger amounts due to improved conversion of EMF over Amberlyst 15 that has higher affinity to water [21]. On the other hand, Nafion NR50, which is a perfluorinated acid resin and thermally stable compared to Amberlyst 15, was tested at 150 °C. The HMF conversion was pretty high as 80.5%, but the yield of EMF (34.2%) was lower than that obtained with Ni_2P/SiO_2-2P along with the formation of DEE, because of the well-known superacidity of Nafion NR50 [25]. The experiment at 180 °C confirmed the stronger acidity of Nafion NR50: the conversion of HMF was 95.7% with the EMF yield of 51.5% and DEE yield of 0.13%. However, since the yields of EMF at 150 and 180 °C were lower than those with Ni_2P/SiO_2-2P, it can be suggested that Ni_2P/SiO_2-2P is a little superior to ion-exchange resin catalysts in terms of the selective formation of EMF. Also, Ni_2P/SiO_2-2P appears to be comparable to the reported Zr-based catalysts [26,27], although the employed reaction conditions are different (Table S1).

Table 1. Activity results in the etherification of HMF [a]

Entry	Catalyst	Alcohol (*R*OH)	BAS/HMF (mol%)	Temperature (°C)	HMF conversion (mol%)	Product selectivity (mol%)		
						EMF	EMFDEA	EL+EF
1	Ni_2P/SiO_2-2P	EtOH	0.07	150	71.2	67.3	14.7	22.0
2	Ni_2P/SiO_2-2P	EtOH	0.07	180	96.5	58.2	23.0	18.8
3	Amberlyst 15	EtOH	0.07	100	53.8	29.4	25.4	45.2
4	Nafion NR50	EtOH	0.07	150	80.5	42.4	19.1	38.5
5	Nafion NR50	EtOH	0.07	180	95.7	53.8	18.5	27.7
6	Ni_2P/SiO_2-2P	EtOH	0.14	150	73.0	56.9	24.1	19.0
7	Ni_2P/SiO_2-2P	EtOH	0.50	150	86.0	48.0	28.3	23.8

[a] Reaction conditions: HMF 4 mmol, alcohol 19 mL, 1 bar N_2, and 3 h.

We further tried verifying the etherification capability of Ni_2P/SiO_2-2P by replacing either HMF or ethanol with different alcohol substrates. The first approach is to react HMF with different primary alcohols such as methanol, 1-propanol, and 1-hexanol. As the reaction pathway in Fig. 2 represents, possible products are 5-(alkoxymethyl)furan (denoted as *R*MF, where *R* is Me, 1-Pr, and 1-Hex representing methyl, propyl, and hexyl, respectively), its acetalization product (*R*MFD*R*A), alkyl levulinate (*R*L), and alkyl formate (*R*F) [26]. In case

of the etherification with methanol at 150 °C and 0.07% BAS/HMF, the conversion of HMF was 90.9% while the selectivity to MeMF plus MeMFDMeA was 58.1%. Among the products, MeF was determined to be the major product (36.8% selectivity), meaning facile transformation of MeMF into MeF via MeL due to the short methyl group. As the alkyl group of alcohols was bulkier, the conversion of HMF decreased to 57.4% for 1-propanol and to 49.4% for 1-hexanol under the identical reaction conditions. However, the selectivity to the etherification products corresponding to *R*MF and *R*MFD*R*A was 63.0% and 67.7% for 1-propanol and 1-hexanol. Therefore, Ni_2P/SiO_2-2P can produce the etherification product in the reaction of HMF with various primary alcohols.

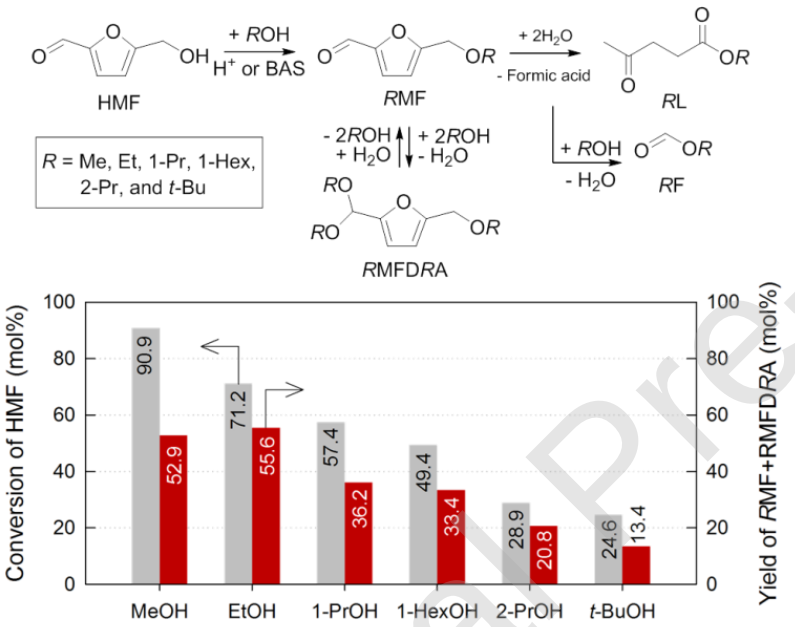

Figure 2. Activities of Ni_2P/SiO_2-2P in the reaction of HMF with various aliphatic alcohols. Reaction conditions: HMF 4 mmol, 0.07% BAS/HMF, alcohol 19 mL, 150 °C, 1 bar N_2, and 3 h.

Furthermore, we tried using branched alcohols as the substrate for the etherification of HMF over Ni_2P/SiO_2-2P (Fig. 2), where the used alcohols are 2-propanol (secondary alcohol) and *tert*-butanol (tertiary alcohol). In case of the etherification of 2-propanol (*R* = 2-Pr) at 150 °C and 0.07% BAS/HMF, the conversion of HMF was 28.9% with the yield of *R*MF plus *R*MFD*R*A at 20.8%. However, only (2-Pr)MFD(2-Pr)A was detected (Fig. S1), because the formation of (2-Pr)MF is favorable at high reaction temperatures. Thus, the increase in reaction temperature to 180 °C resulted in the enhancement in the HMF conversion (83.8%) and (2-Pr)MF yield (26.0%). Additionally, Ni_2P/SiO_2 was tested in the reaction of HMF with *tert*-butanol (*R* = *t*-Bu) at 150 °C. As a result, the HMF conversion was 24.6% and the yield

of *R*MFD*R*A was 13.4% with no formation of *R*MF. Surprisingly, isobutene was produced at the yield of 3.6% (Fig. S1), indicating that Ni_2P/SiO_2 can catalyze the dehydration of *tert*-butanol. The formation of isobutene was also observed using Nafion NR50. Therefore, Ni_2P/SiO_2-2P possibly catalyzes the etherification of HMF with secondary and tertiary alcohols, even if its performance is reduced compared to when primary alcohols are used.

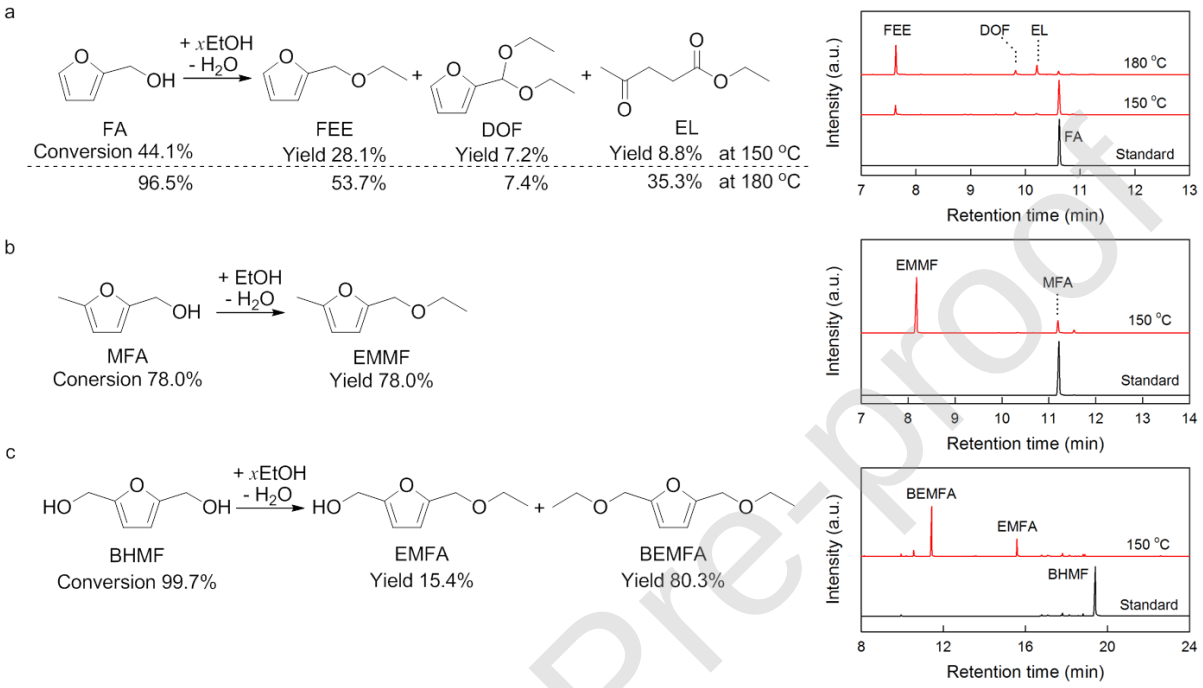

Figure 3. Etherification of furanyl alcohols with ethanol over Ni_2P/SiO_2-2P. a Conversion of furfuryl alcohol (FA) into furfuryl ethyl ether (FEE), 2-(diethoxymethyl)furan (DOF), and EL. **b** Conversion of 5-methylfurfuryl alcohol (MFA) into 2-(ethoxymethyl)-5-methylfuran (EMMF). **c** Conversion of 2,5-bis(hydroxymethyl)furan (BHMF) into 5-(ethoxymethyl)furfuryl alcohol (EMFA) and 2,5-bis(ethoxymethyl)-furan (BEMFA). Reaction conditions: furanyl alcohol 4 mmol, 0.07% BAS/HMF, ethanol 19 mL, 150 °C, 1 bar N_2, and 3 h. To denote the products in the reaction scheme, the gas chromatograms of the product mixtures and substrate are presented in the right-handed side.

The other approach we attempted is to replace HMF with different furanyl alcohols such as furfuryl alcohol (FA), 5-methylfurfuryl alcohol (MFA), and 2,5-bis(hydroxymethyl)furan (BHMF) for the etherification with ethanol. At 150 °C and 0.07% BAS/HMF, Ni_2P/SiO_2-2P transformed FA into furfuryl ethyl ether (FEE) with the selectivity of 63.7% (Fig. 3a). When a high reaction temperature of 180 °C was employed, the conversion of FA increased to 96.5% while the selectivity to FEE was reduced to 55.7% accompanied by the increase in the selectivity to EL (36.6%). The next example is MFA that can react with ethanol to produce 2-(ethoxymethyl)-5-methylfuran (EMMF) [28]. After the etherification over Ni_2P/SiO_2-2P at 150 °C for 3 h, 78.0% of MFA was converted into EMMF with negligible side products (Fig.

3b). The final test was done for BHMF in which the hydroxyl groups on both sides of the furan ring are changed step by step into ether groups; namely, the first etherification product 5-(ethoxymethyl)furfuryl alcohol (EMFA) followed by 2,5-bis(ethoxymethyl)furan (BEMFA) [28]. Surprisingly, 99.7% of BHMF could be converted at 150 °C into EMFA (15.4% yield) and BEMFA (80.3% yield) with several unknown products (Fig. 3c). The superior catalytic performance in the etherification of BHMF is ascribed to the intrinsic ability of electron-donating hydroxyl groups that are symmetrically placed in BHMF. Consequently, Ni_2P/SiO_2-2P can catalyze the etherification of various furanyl alcohols with ethanol, where the reaction efficiency depends on chemical vulnerability of furan structure.

3.2. The acidity of Ni_2P/SiO_2-2P catalyst

X-ray photoelectron spectroscopy (XPS) was performed to distinguish the oxidation states of surface P and Ni species in the Ni_2P/SiO_2-2P catalyst (Fig. 4a). In the Ni 2p core level, the peaks representing divalent Ni (Ni^{2+}) at 857 and 873 eV are detected along with shakeup satellite peaks [29,30]. Another peaks at 853 and 870 eV indicate the presence of $Ni^{\delta+}$ species ($0 < \delta < 1$), which results from the electron density transfer from Ni to P atom in Ni_2P [13,29,31]. All these peaks were confirmed in the spectrum of bulk Ni_2P. In the P 2p region of 140 to 128 ppm, Ni_2P/SiO_2-2P exhibited two peaks at 135.1 and 129.6 eV. The former peak can be assigned as pentavalent P (P^{5+}) since P_xO_y/SiO_2 exhibits only the peak at 135.4 eV. This P^{5+} species is associated with the surplus of the phosphorus added for the preparation of Ni_2P/SiO_2-2P, which will be discussed later. The peak at 129.6 eV represents the presence of partially reduced P species corresponding to $P^{\delta-}$. Therefore, the presence of both $Ni^{\delta+}$ and $P^{\delta-}$ species in the Ni_2P/SiO_2-2P suggests the strong covalent bonding between Ni and P atoms in the supported Ni_2P particles.

The acidity of Ni_2P/SiO_2-2P was examined by pyridine-chemisorbed FT-IR using P_xO_y/SiO_2 and Ni/SiO_2 as a reference material (Fig. 4b). Ni/SiO_2 shows only the absorption bands at 1448 and 1596 cm^{-1}, indicating the presence of Lewis acid sites (LAS). In contrast, only the bands corresponding to the BAS are clearly noticed in the sample P_xO_y/SiO_2. The LAS and BAS were quantitatively calculated using the band areas at 1448 and 1546 cm^{-1}, respectively [32]. As a result, the acid site density of Lewis acidic Ni/SiO_2 is 14.1 μmol g^{-1} and that of Brønsted acidic P_xO_y/SiO_2 is 62.4 μmol g^{-1}. For Ni_2P/SiO_2-2P, the bands for the BAS and LAS are all seen, which is consistent to the results of previous reports [6,33]. The calculated density of BAS (28.0 μmol g^{-1}) is over double that of LAS (11.4 μmol g^{-1}).

Moreover, another footprint by pyridine chemisorption was found in the hydroxyl region of 4000 to 3400 cm^{-1}. Ni_2P/SiO_2-2P shows the negative peaks at 3746 and 3661 cm^{-1} corresponding to the groups of Si–OH and P–OH, respectively. This is supported by the findings on the spectra of Ni/SiO_2 (only Si–OH) and P_xO_y/SiO_2 (both Si–OH and P–OH). Therefore, the group of P–OH in Ni_2P/SiO_2-2P can play the role of Brønsted acidity in the etherification reaction.

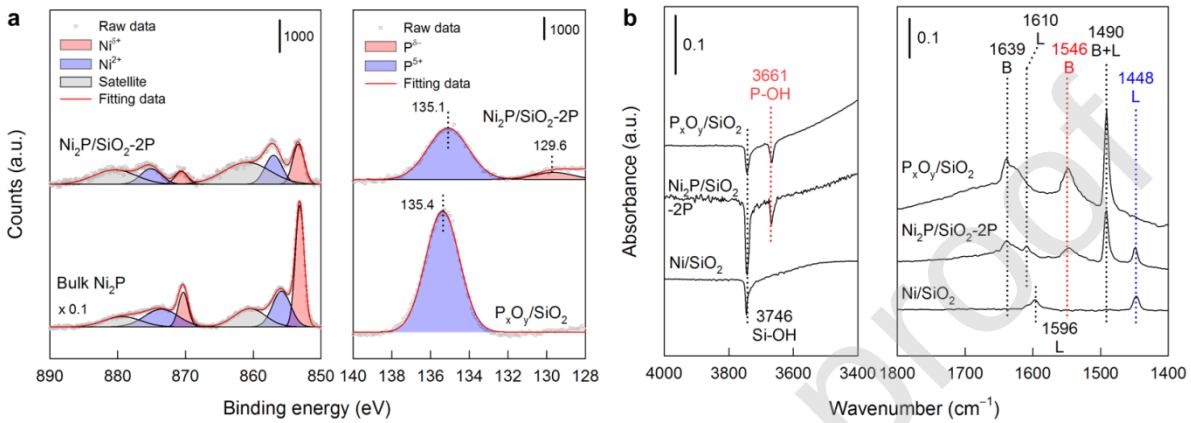

Figure 4. Characterization results of Ni_2P/SiO_2-2P. a XP spectra in the regions of Ni 2p and P 2p, compared to those of P_xO_y/SiO_2 (for P 2p) and bulk Ni_2P (for Ni 2p). **b** Pyridine-chemisorbed FT-IR spectrum, compared to those of P_xO_y/SiO_2 and Ni/SiO_2.

The phase of Ni_2P in the prepared Ni_2P/SiO_2-2P was confirmed by the standard reflections of Ni_2P (PDF #03-0953) and X-ray diffraction (XRD) peaks of unsupported (or called bulk) Ni_2P particles (Fig. 5a). Using the Ni_2P (111) reflection at 2θ of 40.8°, the size of Ni_2P particles in Ni_2P/SiO_2 was calculated to be 23.1 nm that is much smaller compared to bulk Ni_2P (49.2 nm). The major planes of Ni_2P phase such as (111) and (201) were identified in the selected area electron diffraction (SAED) patterns of TEM image (Fig. 5b). This is the reason why the Ni_2P/SiO_2-2P with the nominal P/Ni molar ratio of 2 was prepared in this work. However, elemental analysis revealed that the actual P/Ni molar ratio was 1 (11.0 wt% for Ni and 5.8 wt% for P), in which the difference between the nominal and actual values is caused by loss of volatile phosphorus in the TPR process to form the Ni_2P phase. This explains that the surplus phosphorus species can exist on the surface of Ni_2P/SiO_2-2P, when considering the theoretical P/Ni ratio of 0.5 in Ni_2P.

To understand the acidity of Ni_2P/SiO_2-2P, we prepared Ni_2P/SiO_2-0.5P and Ni_2P/SiO_2-1P of which the actual P/Ni molar ratio was measured to be 0.5 and 0.9, respectively (Table 2). The XRD patterns of these samples show that the peaks corresponding to $Ni_{12}P_5$ phase are more intense with the decrease in the P/Ni ratio along with the peaks of Ni_2P phase (Fig. 5a).

This is consistent to the previous reports in which $Ni_{12}P_5$ is transformed into Ni_2P as the P/Ni ratio increases [8,34]. Therefore, when the P/Ni molar ratio is close to the theoretical value of Ni_2P, the major phase of supported nickel phosphide is $Ni_{12}P_5$ and not Ni_2P.

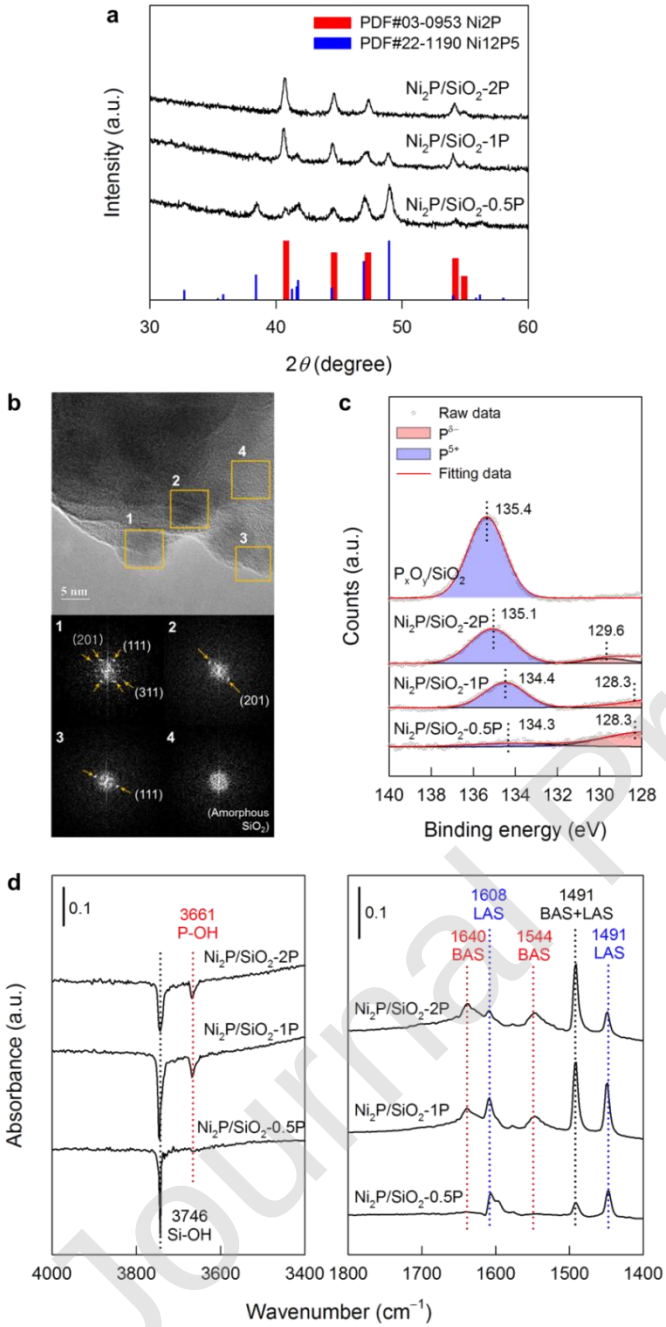

Figure 5. Characterization results of Ni_2P/SiO_2-*x*P (*x* = 0.5, 1, and 2). a XRD patterns. **b** TEM image of Ni_2P/SiO_2-2P in the scale bar of 5 nm and SAED patterns of Ni_2P phase (1–3) and amorphous SiO_2 (4). **c** XP spectra in the region of P 2p, compared to those of P_xO_y/SiO_2. **d** Pyridine-chemisorbed FT-IR spectra. For comparison, the results of Ni_2P/SiO_2-2P are reproduced herein.

Table 2. Compositions of Ni and P in Ni_2P/SiO_2-*x*P, Ni/SiO_2, and P_xO_y/SiO_2

Catalyst	Actual composition (wt%) [a]		Actual P/Ni ratio	Surface composition (at%) [b]		Surface P/Ni ratio	Area percentage of P species [c]	
	Ni	P		Ni	P		P^{5+}	$P^{\delta-}$
Ni/SiO_2	10.3	-	-	0.27	-	-	-	-
Ni_2P/SiO_2-0.5P	12.1	3.1	0.5	0.51	0.22	0.4	19	81
Ni_2P/SiO_2-1P	10.6	5.2	0.9	0.52	1.14	2.2	58	42
Ni_2P/SiO_2-2P	11.0	5.8	1.0	0.56	1.84	3.3	88	12
P_xO_y/SiO_2	-	9.3	-	-	6.95	-	100	0

[a] Measured by ICP-AES analysis. [b] Measured by XPS analysis. [c] Calculated by peak area in Fig. 5c.

XP spectra in the region of P 2p were compared to notice the difference in the environment of phosphorus (Fig. 5c). As the P/Ni ratio decreases from 2 to 0.5, the peak of P^{5+} becomes weak and is gradually shifted to 134.3 eV, meaning the disappearance of phosphate group. On the contrary, the peak of $P^{\delta-}$ grows up with the P/Ni ratio decreasing: the area percentage of $P^{\delta-}$ increases from 12% for Ni_2P/SiO_2-2P to 81% for Ni_2P/SiO_2-0.5P (Table 2). This possibly suggests that 81% of the P species present in Ni_2P/SiO_2-0.5P takes parts in the formation of Ni–P bond whereas 88% of the P species in Ni_2P/SiO_2-2P exists in the form of phosphate group. In other words, the surplus phosphorus is required to produce the phase of Ni_2P in Ni_2P/SiO_2-2P but the P species left after forming the Ni–P bond is used for the phosphate group.

The surface compositions measured by XPS are listed in Table 2. For Ni_2P/SiO_2-*x*P, the surface composition of Ni is similar at around 0.5 at% whereas that of P increases from 0.22 to 1.84 at% with the *x* value increasing. Hence, the surface P/Ni molar ratio increases in the following order: 0.4 (Ni_2P/SiO_2-0.5P) < 2.2 (Ni_2P/SiO_2-1P) < 3.3 (Ni_2P/SiO_2-2P). More importantly, the surface P/Ni molar ratios in the latter two catalysts are higher than the actual values. This implies that the surplus P species is more located on the surface for Ni_2P/SiO_2-1P and Ni_2P/SiO_2-2P. According to the literature [7,35,36], the surplus P species, including the unreduced phosphate (such as $H_nPO_4^{(3-n)-}$, $P_2O_7^{4-}$, and $(PO_3^-)_n$) and the element P (such as P_2 and P_4), may locate on the surfaces of Ni_2P particles and/or SiO_2 support. These species as well as the P species on the Ni_2P particle surface can be combined with the water formed during the TPR process employed for catalyst preparation, leading to the formation of the P–OH group [35–37].

The densities of the BAS and LAS in Ni_2P/SiO_2-*x*P and P_xO_y/SiO_2 were measured by pyridine-chemisorbed FT-IR analysis (Fig. 5d and Table 3). The density of BAS increases in the following order: 0.0 (Ni/SiO_2) < 1.9 (Ni_2P/SiO_2-0.5P) < 22.3 (Ni_2P/SiO_2-1P) < 28.0 (Ni_2P/SiO_2-2P) < 62.4 μmol g^{-1} (P_xO_y/SiO_2). The BAS densities of Ni_2P/SiO_2-1P and

Ni_2P/SiO_2-2P can be explained by the surplus P species. In contrast, Ni_2P/SiO_2-0.5P contains the very little density of BAS compared to that of LAS (14.0 μmol g^{-1}), while it shows the very small peak of P–OH group ascribed to 3661 cm^{-1}. This suggests that as the actual P/Ni ratio is close to the theoretical value, an ideal Ni_2P/SiO_2 would be Lewis acidic though a very little BAS can still exist on the surface of Ni_2P particles. However, it should be noted here that Ni_2P/SiO_2-0.5P exhibits the phases of both Ni_2P and $Ni_{12}P_5$ with the latter being in major (according to its XRD pattern). In this respect, the higher LAS density in Ni_2P/SiO_2-1P compared to Ni_2P/SiO_2-0.5P can be rationalized by the fact that the latter sample has abundant Ni_2P phase. Because of this feature, the surplus P species added for Ni_2P/SiO_2-1P may exist in the form of the unreduced phosphate (i.e., the P–OH group corresponding to the BAS) that mainly locates on the surface of SiO_2 support. This explanation is also reasonable for the higher BAS density of Ni_2P/SiO_2-2P. Furthermore, the surplus P species would be located as the form of the element P on the surface of Ni_2P particles, as suggested in Chen et al. [35]. This is corroborated by the considerably reduced density of LAS is in Ni_2P/SiO_2-2P. Besides, the molar ratio of BAS to LAS increases with the P/Ni ratio in the order: 0.14 (Ni_2P/SiO_2-0.5P) < 0.83 (Ni_2P/SiO_2-1P) < 2.46 (Ni_2P/SiO_2-2P). Such a ratio is consistent to the fraction of surface P^{5+} species. Consequently, the P–OH group could be located on the surface of Ni_2P particles and SiO_2 support, as suggested in the previous report [35].

Table 3. Activity results in the etherification of HMF with ethanol over Ni/SiO_2, P_xO_y/SiO_2, and Ni_2P/SiO_2-*x*P [a] and catalyst acidity

Catalyst	HMF conversion (mol%)	EMF yield (mol%)	Product selectivity (mol%)			Acidity (μmol g^{-1}) [e]	
			EMF	EMFDEA	EL+EF	BAS	LAS
Ni/SiO_2 [b]	25.6	5.4	20.9	10.8	68.3	–	14.1
Ni_2P/SiO_2-0.5P [c]	43.0	17.7	41.1	21.2	37.7	1.9	14.0
Ni_2P/SiO_2-1P [c]	56.5	38.0	67.3	12.2	16.7	22.3	26.8
Ni_2P/SiO_2-2P [c,d]	68.9	46.4	67.3	11.7	21.0	28.0	11.4
P_xO_y/SiO_2 [d]	74.5	54.0	72.5	8.1	19.4	62.4	–

[a] Reaction conditions: HMF 4 mmol, ethanol 19 mL, 150 °C, 1 bar N_2, 600 rpm, and 3 h. [b] 0.07 mol% LAS/HMF. [c] Catalyst 0.1 g. [d] 0.07 mol% BAS/HMF. [e] Calculated by the spectra shown in Fig. 5d.

Ni_2P/SiO_2-*x*P, Ni/SiO_2, and P_xO_y/SiO_2 were tested in the etherification of HMF with ethanol. Table 3 lists the detailed activity results and Fig. 6 presents the HMF conversion and EMF yield with the densities of the BAS and LAS. The blank test at 150 °C showed the HMF conversion of ca. 12% with the EMF yield of 2.6%. In the case of Ni/SiO_2 possessing only the LAS, the HMF conversion and EMF yield are estimated to be 25.6% and 5.4%, respectively. In contrast, Brønsted acidic P_xO_y/SiO_2 presents the high HMF conversion (74.5%) and EMF yield (54.0%), which is similar to the activity result (HMF conversion =

77.4% and EMF yield = 47.3%) of SiO_2-supprted nickel phosphate corresponding to the precursor of Ni_2P/SiO_2-2P. The HMF conversion of Ni_2P/SiO_2-*x*P increases with the P/Ni ratio in the following order: 43.0% (Ni_2P/SiO_2-0.5P) < 56.5% (Ni_2P/SiO_2-1P) < 68.9% (Ni_2P/SiO_2-2P).

First, we suggest that the HMF etherification can proceed not only over the BAS but also over the LAS, because Ni/SiO_2 and Ni_2P/SiO_2-0.5P show a little activity even if the BAS is absent in the former and very low in the latter. Next, the contribution of the BAS to the activity is more significant than that of the LAS, when considering the catalytic performance of P_xO_y/SiO_2 and Ni_2P/SiO_2-2P. The last finding is associated with the result that the HMF conversion and EMF yield are relatively similar with P_xO_y/SiO_2 and Ni_2P/SiO_2-2P though the BAS density of the former is 2.2-fold higher than that of the latter. Lee and Oyama reported that the P–OH group ascribed to the BAS was stronger for P_xO_y/SiO_2 compared with Ni_2P/SiO_2 [6]. Li et al. found from NH_3-TPD profiles that the Lewis acidity on Ni_2P/SiO_2 was stronger than the Brønsted acidity on P_xO_y/SiO_2 [38] and bulk Ni_2P [39]. Form these reports, we can presume that the comparable activity between P_xO_y/SiO_2 and Ni_2P/SiO_2-2P is attributed to the stronger Lewis acidity of Ni_2P/SiO_2-2P. Consequently, it is believed that both Brønsted and Lewis acidities of Ni_2P/SiO_2-2P are responsible for the etherification activity.

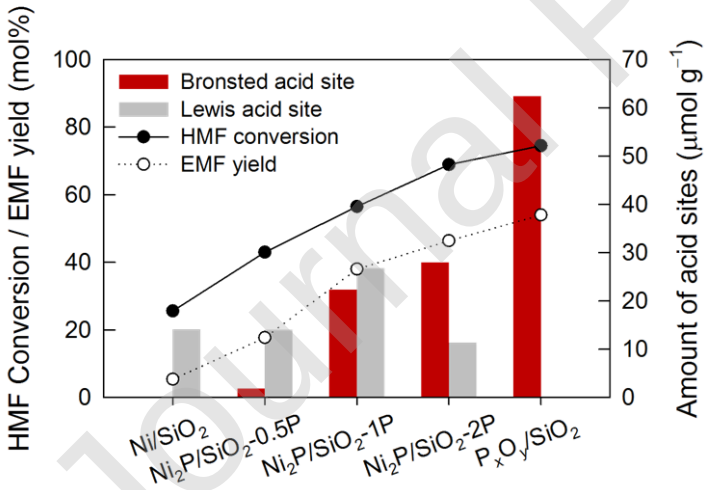

Figure 6. Relation between the etherification activity and acidity of Ni/SiO_2, P_xO_y/SiO_2, and Ni_2P/SiO_2-*x*P.

3.3. Recyclability of Ni_2P/SiO_2-2P catalyst in the etherification of HMF with ethanol

The recyclability of Ni_2P/SiO_2-2P was confirmed by repeated use in the etherification of HMF with ethanol, where the reaction temperature of 180 °C was selected so as to clearly identify the transformation of the active Ni_2P phase. In Fig. 7a the catalytic first-run activity

of Ni_2P/SiO_2-2P is displayed as a single bar representing the yields of all the formed products (using the same values given in Fig. 1d). The spent Ni_2P/SiO_2-2P was obtained after washing with the ethanol solvent without post heat-treatment. As a result, the HMF conversion decreased a little to 89.2% and 86.8% in the second and third runs, respectively. Meanwhile, the EMF yield was reduced to 57.5% and 52.4% in the recycle runs. Since the observed activity loss may be related with the transformation of Ni_2P phase, the spent Ni_2P/SiO_2 obtained after the first run was regenerated by H_2 reduction at 700 °C for 1 h. As a result, both the HMF conversion and EMF yield could be recovered to 95.7% and 63.3%, respectively, which are comparable to the performance of the fresh Ni_2P/SiO_2-2P.

The spent Ni_2P/SiO_2-2P catalysts were characterized by the aforementioned techniques. Their XRD patterns show that the intensities of Ni_2P reflections in the spent samples are not changed considerably (Fig. 7b). This suggests that the Ni_2P phase in the bulk is possibly preserved in the course of the etherification reaction. Nonetheless, it should be noted that the peak at 2θ of 26.6° corresponding to the elemental carbon (PDF #03-0953) was detected, which indicates the formation of coke species during the reaction. This coke formation can result from the high reactivity of HMF at high temperatures producing humin [40].

We further characterized the spent and regenerated Ni_2P/SiO_2-2P samples (obtained after the first activity run and after H_2 reduction of the spent catalyst at 700 °C, respectively) to compare with the fresh one. The XP spectrum of the spent Ni_2P/SiO_2-2P shows that in the region of Ni 2p, the peaks corresponding to $Ni^{\delta+}$ species are reduced and, in turn, the peaks of Ni^{2+} are enlarged, while the peak of $P^{\delta-}$ species also decreases in the P 2p region (Fig. 7c). This suggests that the oxidation of Ni_2P particles during the reaction. Since the instability of the Ni_2P phase in high-temperature water was reported previously [12], another spent catalyst sample was prepared by exposing Ni_2P/SiO_2-2P into pure ethanol under the reaction conditions. The XP spectrum of this sample exhibits that the species of $Ni^{\delta+}$ and $P^{\delta-}$ are maintained (Fig. S2). Therefore, water molecules produced by the etherification reaction can induce the oxidation of Ni_2P surface and formation of P–OH group, assuming the increase in the Brønsted acidity. Nevertheless, the BAS density in the spent Ni_2P/SiO_2-2P decreased to 18.0 μmol g^{-1}, although the compositions of Ni and P in the spent catalysts were not largely different from those in the fresh one (Table S2). This indicates that the formed coke (examined by XRD analysis) might be responsible for the activity loss in repeated runs. However, the characteristics of the regenerated Ni_2P/SiO_2-2P were similar to those of the

fresh one even though a little discrepancy was observed in the XPS results. This suggests that the regeneration we employed can fully recover the catalytic performance of Ni_2P/SiO_2-2P.

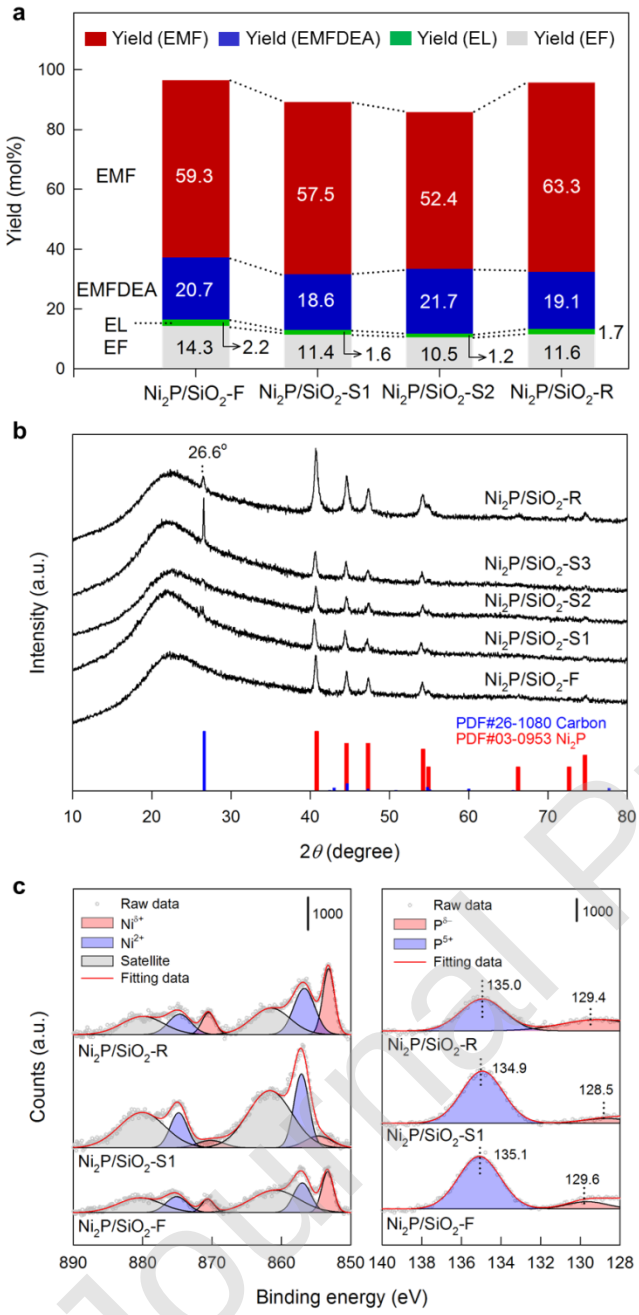

Figure 7. Recyclability of Ni_2P/SiO_2-2P catalyst in the etherification of HMF with ethanol. a Activity results over the fresh catalyst (Ni_2P/SiO_2-F), the spent catalysts (Ni_2P/SiO_2-S1 and Ni_2P/SiO_2-S2 obtained after the first and second reaction runs, respectively), and the regenerated catalyst (Ni_2P/SiO_2-R obtained after H_2 reduction of Ni_2P/SiO_2-S1 at 700 °C). Reaction conditions: catalyst 100 mg, HMF 4 mmol, ethanol 19 mL, 180 °C, 1 bar N_2, and 3 h. **b** XRD patterns of Ni_2P/SiO_2-F, Ni_2P/SiO_2-S1, Ni_2P/SiO_2-S2, Ni_2P/SiO_2-S3 (obtained after the third reaction run), and Ni_2P/SiO_2-R. **c** XP spectra of Ni_2P/SiO_2-F, Ni_2P/SiO_2-S1, and Ni_2P/SiO_2-R in the regions of Ni 2p and P 2p.

4. Conclusion

We herein demonstrated the capability of a SiO_2-supported Ni_2P catalyst in the etherification of furanyl alcohols with aliphatic alcohols under inert atmosphere. All the activity tests disclosed that the Ni_2P/SiO_2 prepared with the nominal P/Ni ratio of 2 (namely, Ni_2P/SiO_2-2P) could produce the etherification products (e.g., EMF and EMFDEA in the reaction of HMF with ethanol) at a fairly good yield. The examined etherification activity was attributed to both Brønsted and Lewis acidity of Ni_2P/SiO_2-2P that was much better than the Lewis acidic Ni/SiO_2 and comparable to the Brønsted acidic P_xO_y/SiO_2. In Ni_2P/SiO_2-2P, the Lewis acid sites was related with Ni species while the Brønsted acid site ascribed to the P–OH group could be located on the surface of Ni_2P particles and SiO_2 support. The catalyst recyclability tests revealed the activity loss due to coke formation but the catalytic performance was fully recovered after regeneration by high-temperature H_2 reduction. Consequently, we suggest that Ni_2P/SiO_2 can catalyze the etherification reaction demanding the acidity only if the actual P/Ni ratio is above the theoretical value so that the Brønsted acid site is sufficiently created. This study will greatly contribute to understanding the acidity of supported Ni_2P catalysts examined in hydrotreating reactions.

Credit author statement

Mi Shin: Methodology, Validation, Formal Analysis, Investigation, Data Curation, Writing – Original Draft, Visualization. **Jinsung Kim:** Formal Analysis, Investigation. **Young-Woong Suh:** Conceptualization, Supervision, Project Administration, Writing – Review and Editing, Funding Acquisition.

Declaration of interests

The authors declare that they have no known competing financial interests or personal relationships that could have appeared to influence the work reported in this paper.

Acknowledgements

This work was financially supported by the Next Generation Carbon Upcycling Program

through the National Research Foundation of Korea (NRF) funded by the Ministry of Science and ICT, Republic of Korea (2017M1A2A2043148). We acknowledge technical supports from the Hanyang LINC+ Analytical Equipment Center in Seoul.

Notes and references

[1] N. P. Sweeny, C. S. Rohrer, O. W. Brown, J. Am. Chem. Soc. 80 (1958) 799–800.

[2] J. L. Wagner, E. Jones, A. Sartbaeva, S. A. Davis, L. Torrente-Murciano, C. J. Chuck, V. P. Ting, Dalton Trans. 47 (2018) 1189–1201.

[3] M. V. Landau, M. Herskowitz, T. Hoffman, D. Fuks, E. Liverts, D. Vingurt, N. Froumin, Ind. Eng. Chem. Res. 48 (2009) 5239–5249.

[4] J. A. Cecilia, A. Infantes-Molina, E. Rodríguez-Castellón, A. Jiménez-López, S. T. Oyama, Appl. Catal. B 136–137 (2013) 140–149.

[5] M. E. Bussell, React. Chem. Eng. 2 (2017) 628–635.

[6] Y.-K. Lee, S. T. Oyama, J. Catal. 239 (2006) 376–389.

[7] S. T. Oyama, Y.-K. Lee, J. Catal. 258 (2008) 393–400.

[8] S. T. Oyama, X. Wang, Y.-K. Lee, K. Bando, F. G. Requejo, J. Catal. 210 (2002) 207–217.

[9] S. Wu, P. Lai, Y. Lin, H. Wan, H. Lee, Y. Chang, ACS Sustainable Chem. Eng. 1 (2013) 349−358.

[10] X. Lan, E. J. M. Hensen, Th. Weber, Appl. Catal. A 550 (2018) 57–66.

[11] L. Ding, A. Wang, M. Zheng, T. Zhang, ChemSusChem 3 (2010) 818–821.

[12] P. Yang, H. Kobayashi, K. Hara, A. Fukuoka, ChemSusChem 5 (2012) 920–926.

[13] C. P. Jiménez-Gómez, J. A. Cecilia, R. Moreno-Tost, P. Maireles-Torres, ChemCatChem 9 (2017) 2881–2889.

[14] Y. Wang, F. Liu, H. Han, L. Xiao, W. Wu, ChemistrySelect 3 (2018) 7926–7933.

[15] J. Jeong, C. A. Antonyraj, S. Shin, S. Kim, B. Kim, K.-Y. Lee, J. K. Cho, J. Ind. Eng. Chem. 19 (2013) 1106–1111.

[16] I. K. Yu, D. C. W. Tsang, Bioresource Technol. 238 (2017) 716–732.

[17] S. Alipour, H. Omidvarborna, D.-S. Kim, Renew. Sust. Energ. Rev. 71 (2017) 908–926.

[18] H. Shi, J. Chen, Y. Yang, S. Tian, Fuel Process. Technol. 118 (2014) 161–170.

[19] Y.-B. Huang, M.-Y. Chen, L. Yan, Q.-X. Guo, Y. Fu, ChemSusChem 7 (2014) 1068–1070.

[20] D. P. Duarte, R. Martínez, L. J. Hoyos, Ind. Eng. Chem. Res. 55 (2016) 54–63.

[21] M. Balakrishnan, E. R. Sacia, A. T. Bell, Green Chem. 14 (2012) 1626–1634.

[22] H. Wang, T. Deng, Y. Wang, X. Cui, Y. Qi, X. Mu, X. Hou, Y. Zhu, Green Chem. 15 (2013) 2379–2383.

[23] M. M. Antunes, P. A. Russo, P. V. Wiper, J. M. Veiga, M. Pillinger, L. Mafra, D. V. Evtuguin, N. Pinna, A. A. Valente, ChemSusChem 7 (2014) 804–812.

[24] M. Musolino, M. J. Ginés-Molina, R. Moreno-Tost, F. Arico, ACS Sustainable Chem. Eng. 7 (2019) 10221–10226.

[25] S. Pariente, N. Tanchoux, F. Fajula, Green Chem. 11 (2008) 1256–1261.

[26] P. Lanzafame, D. M. Temi, S. Perathoner, G. Centi, A. Macario, A. Aloise, G. Giordano, Catal. Today 175 (2011) 435–441.

[27] M. M. Antunes, S. Lima, P. Neves, A. L. Magalhães, E. Fazio, F. Neri, M. T. Pereira, A. F. Silva, C. M. Silva, S. M. Rocha, M. Pillinger, A. Urakawa, A. A. Valente, Appl. Catal. B 182 (2016) 485–503.

[28] E. R. Sacia, M. Balakrishnan, A. T. Bell, J. Catal. 313 (2014) 70–79.

[29] P. Bui, J. A. Cecilia, S. T. Oyama, A. Takagaki, A. Infantes-Molina, H. Zhao, E. Rodríguez-Castellón, A. J. López, J. Catal. 294 (2012) 184–198.

[30] L. Gua, Y. Zhao, Z. Yao, Dalton Trans. 45 (2016) 1225–1232.

[31] S. J. Sawhill, D. C. Phillips, M. E. Bussell, J. Catal., 215 (2003) 208–219.

[32] C. A. Emeis, J. Catal. 141 (1993) 347–354.

[33] S. T. Oyama, T. Gott, K. Asakura, S. Takakusagi, K. Miyazaki, Y. Koike, K. K. Bando, J. Catal. 268 (2009) 209–222.

[34] V. O. O. Goncalves, P. M. Souza, T. de Cabioc'h, V. T. da Silva, F. B. Noronha, F. Richard, Catal. Comm. 119 (2019) 33–38.

[35] J. Chen, T. Guo, K. Li, L. Sun, Catal. Sci. Technol. 5 (2015) 2670–2680.

[36] C. Stinner, Z. Tang, M. Haouas, Th. Weber, R. Prins, J. Catal. 208 (2002) 456–466.

[37] S. T. Oyama, T. Gott, H. Zhao, Y. Lee, Catal. Today 143 (2009) 94–107.

[38] K. Li, R. Wang, J. Chen, Energy. Fuels 25 (2011) 854–863.

[39] Y. Wang, X. Feng, S. Yang, L. Xiao, W. Wu, J. Nanopart. Res. 22 (2020) 67.

[40] M. Schlaf, Z.C. Zhang, Reaction pathways and mechanisms in thermocatalytic biomass conversion I, first ed., Springer, Singapore, 2016.